

Memristive Fingerprints of Electric Arcs

Wieslaw Marszalek
DeVry University, 630 US Highway 1
North Brunswick, NJ 08902, USA
email: wmarszalek@devry.edu

January 8, 2016

Abstract

We discuss the memristive fingerprints of the hybrid Cassie-Mayr model of electric arcs. In particular, it is shown that (i) the voltage-current characteristic of the model has the pinched hysteresis nature, (ii) the voltage and current zero crossings occur at the same instants, and (iii) when the frequency f of the power supply increases, the voltage-current pinched hysteresis characteristic tends closer to a single-valued one, meaning that the voltage-current graph becomes that of a resistor (with an increased linearity for $f \rightarrow \infty$). The conductance g of the Cassie-Mayr model decreases when the frequency increases. The hybrid Cassie-Mayr model describes therefore an interesting case of a memristive phenomenon.

1 Introduction

Consider the Cassie-Mayr hybrid model of electric arcs [1]-[12]

$$g = G_{min} + \left[1 - e^{-\frac{i^2}{I_0^2}} \right] \frac{ui - Ki^2}{U_C^2} + e^{-\frac{i^2}{I_0^2}} \frac{i^2}{P_M} - \theta \frac{dg}{dt} \quad (1)$$

driven by a power circuit with the voltage source $E(t) = E_m \sin(2\pi ft)$, resistor R and inductor L , described by

$$L \frac{di}{dt} + Ri + u = E \quad (2)$$

where u and i are the arc voltage and current, respectively, g is the conductance of the arc with $u = i/g$ and G_{min} , I_0 , K , U_C , P_M , L , R , E_m , f are real positive constants, $\theta = \theta_0 + \theta_1 e^{-\alpha|i|}$, with θ_0 , θ_1 and α being constants such that $\theta_0 \ll \theta_1$. When the current i is small, one can consider $\theta \approx \theta_1$, while for large current $\theta \approx \theta_0$ [3]. Another frequent simplification (however not assumed in this paper) is to have $K = 0$, which means that no energy dissipation occurs due to plasma radiation.

Also, the positive constant G_{min} plays the role of a minimum value of $g(t)$, as many authors assume that $g(t) > G_{min}$ when the current $i(t)$ is small. The G_{min} is a very small conductance between two electrodes when the arc is absent. In general, the value of G_{min} depends on the distance between the electrodes, their geometry, type of gas used and temperature. Detailed physical assumptions about the above model can be found, for example, in [3]-[7].

The literature on electric arcs in welding, foundry, gas discharge lamps, lighting as well as voltaic, iron, cobalt, nickel, titanium and mercury arcs is particularly immense over the last 150 years. For example, many papers on electric arcs were published in the Journal of the Franklin Institute over a period of more than hundred years - since 1850s to 1950s - see [8]-[12] for a few examples of such papers. A list of papers on the topic of electric arcs available in the literature can really be made impressive and long.

Impressive are also the very recent discoveries in the area of nanotechnology related to memristors and memristive circuits and their properties. The announcement by a group of Hewlett Packard researchers [13] about a successful construction of 'the missing memristor' renewed interest in the earlier theoretical work of L. O. Chua and others on memristors [14],[15]. That research has been significantly expanded in the last few years, see [16]-[23] and references therein.

The two seemingly distant areas of electric arcs and memristors are, in fact, close to each other and this paper addresses that issue through the analysis of the properties of the models of electric arcs and the models of memristors.

In particular, it is shown in this paper that the model (1),(2) has the three fingerprints of memristors (see [16],[18],[19]), as follows:

- The u and i characteristic is of the pinched hysteresis type.
- The u and i zero crossings occur at the same instants.
- As $f \rightarrow \infty$, then the u - i pinched hysteresis characteristic becomes that of a resistor, meaning that the u - i graph is a single-valued one with no memory effect.

The above fingerprints are illustrated in Fig.1(a)-1(c) for a selected set of constant parameters in (1) and (2).

2 Memristors

Memristors, as passive elements, complement the widely used other passive elements: resistors, capacitors and inductors. Each of the four passive two-port elements uses a pair of the current, voltage, charge or flux variables as their inputs and outputs. Memristors are nonlinear elements whose present state at any instant depends on the past (i.e. memory). For example, the current-controlled voltage memristor is described by a relationship between the flux $\phi(t)$ and charge $q(t)$, as follows: $\phi(t) = F(q(t))$ with some function $F \in C^1$. This gives the Ohm's law for such a memristor in the form: $u(t) = r(\int i(t)dt)i(t)$, with $r(q) = dF(q)/dq$, the memristance, while $u(t)$ and $i(t)$ denote the voltage and current, respectively. The memory effect is due to the dependence of memristance r on $\int i(t)dt$. Other types of mem-elements are also possible (see [17] and references therein). The recent papers [16],[18]-[20] show interesting electrical, mechanical and biological devices and phenomena, all having the features (the so-called fingerprints) of memristors. This paper goes in the same direction and proves mathematically that the hybrid Cassie-Mayr model of an electric arc [3] has the three fingerprints of memristors (in the time- and frequency domains).

First, it is worth pointing out that the fundamental idea behind the model (1),(2) is to have the conductance $g(t)$ as a combination of the conductances $g_C(t)$ and $g_M(t)$, as follows [4],[24]

$$g(t) = [1 - \sigma(i(t))]g_C(t) + \sigma(i(t))g_M(t) \quad (3)$$

where g_C and g_M are the conductances obtained from the Cassie and Mayr models, respectively, and the weighting function $0 \leq \sigma(i) \leq 1$ is monotonically increasing when $i(t)$ increases. Also, typically $\sigma(0) = 1$. The most common choice is to have $\sigma(i) = e^{-i^2/I_0^2}$ in (1), with $I_0 = \text{const}$ being the *transition* current. When $i(t)$ is much smaller than I_0 , the Mayr model is dominant in (1), while for $i(t)$ large, the Cassie model dominates in (1). This feature of the hybrid Cassie-Mayr model is similar to that of the Hewlett Packard (HP) memristor's model in which the total memristance is obtained as a weighted sum of R_{OFF} and R_{ON} resistances [13]

$$R(t) = \left[1 - \frac{w(t)}{D}\right] R_{OFF}(t) + \frac{w(t)}{D} R_{ON}(t) \quad (4)$$

where R_{ON} and R_{OFF} denote the resistances of the region with a high concentration of dopants (having low resistance R_{ON}), and the region with a low dopant concentration (having much higher resistance R_{OFF}), respectively. Thus, $R_{ON} \ll R_{OFF}$ and $0 \leq w(t) \leq D$. As a consequence, we have a one-to-one correspondence between (3) and (4). Namely, $w(t) \ll D$ gives $R(t) \approx R_{OFF}$ resulting in a *small* memristor's current. A *small* $i(t)$, that is $i(t) \ll I_0$ in an electric arc, gives $g(t) \approx g_M$. On the other hand, $w(t)$ close to D yields $R(t) \approx R_{ON}$ and a *large* memristor's current. A *large* $i(t)$, that is $i(t) \gg I_0$ in an arc, results in $g(t) \approx g_C$.

The $\sigma(i) = e^{-i^2/I_0^2}$ used in (3) is not the only possible function used in hybrid arc models. Other monotonical functions $\sigma(i(t))$ used in modeling of electric arcs are $e^{-\left(\frac{|i|}{I_0}\right)^a}$, $e^{-\left(\frac{|i|}{I_0}\right)^{a/(\delta+|i|)}}$ or $1/[1 + e^{\beta(|i|-I_0)}]$ for constants a , δ and β [24].

The above one-to-one correspondence between an electric arc and a memristor is further obvious by analyzing the three fingerprints of memristive phenomena, mentioned above and analyzed in detail in the next section.

3 The three memristive fingerprints of electric arcs

Fingerprint 1: The u - i characteristic of (1),(2) is of the pinched hysteresis type.

Remark 1: The pinched property occurs at the origin, so $u \approx 0$ and $i \approx 0$. By using $u = i/g$ and the fact that the pinched property occurs at $i \rightarrow 0$, it is possible to show that du/di in (1),(2) has **one** positive value as $u \rightarrow 0$ and $i \rightarrow 0$, but d^2u/di^2 has **two** different values (positive and negative) at the origin. The two opposite values of d^2u/di^2 occur half a period apart (see Fig.2(a)). This indicates that there are **two** different trajectories of the u - i characteristic at the origin, one that is concave up (with $d^2u/di^2 > 0$) and another that is concave down (with $d^2u/di^2 < 0$). See Fig.2(b) showing clearly **two** tangential trajectories with different concavity around the origin.

Proof of fingerprint 1: Notice that the pinched hysteresis occurs as $i \rightarrow 0$. Thus, the Mayr model is in effect. Let $u(t_*) = 0$ and $i(t_*) = 0$ (see the second fingerprint below). We have $g(t_*) > 0$. Also, since $u = i/g$, therefore we have $du/dt = [(di/dt)g - (dg/dt)i]/g^2 = (di/dt)/g$ when $i = 0$. This yields $du/di = 1/g$. At $t = t_*$ we have $du/dt = (di/dt)/g(t_*)$, and since $g(t_*) > 0$, therefore $du/di|_{t_*} > 0$. Thus, the pinched hysteresis has slope $1/g(t_*)$ at $(u, i) = (0, 0)$.

Now, we shall show that d^2u/di^2 is a two-valued quantity at $(u, i) = (0, 0)$, that is $d^2u/di^2|_{t_*}$ and $d^2u/di^2|_{t_*+T/2}$ are of opposite signs. Using the fact that $i = 0$ yields $du/di = 1/g$, we obtain $d^2u/di^2 = -(dg/di)/g^2 = -(1/g^2)(dg/dt)/(di/dt)$. Note that the derivative dg/dt is positive at $t = t_*$ and also from (2) we have $di/dt|_{t_*} = (E_m/L)\sin(2\pi ft_*)$, since $i(t_*) = 0$ and $u(t_*) = 0$. Thus, the Mayr model predicts that when the periodic, zero-average current $i(t)$ crosses the zero value at $t = t_*$, it is of a cosine type, with opposite signs of slope at $t = t_*$ and $t = t_* + T/2$. If $di/dt|_{t_*} > 0$, then, half a period later we have $di/dt|_{t_*+T/2} < 0$. This yields $d^2u/di^2|_{t_*} < 0$ and $d^2u/di^2|_{t_*+T/2} > 0$. On the other hand, if $di/dt|_{t_*} < 0$, then, half a period later we have $di/dt|_{t_*+T/2} > 0$. This yields $d^2u/di^2|_{t_*} > 0$ and $d^2u/di^2|_{t_*+T/2} < 0$. This proves that the concavity of the trajectory (pinched hysteresis) is opposite at $t = t_*$ than at $t = t_* + T/2$. The trajectory moving in time along the u - i characteristic is of different type of concavity when passing through $u = 0, i = 0$ every half of the period T , as illustrated in Figs.2(a) and 2(b). This completes the proof of the first memristive fingerprint of the hybrid Cassie-Mayr model. \diamond

The facts that the slope du/di has the same positive value at $t = t_*$ and at $t = t_* + T/2$ and opposite values of d^2u/di^2 at $t = t_*$ and $t = t_* + T/2$ yield the pinched hysteresis of type II, as discussed in [25]-[27].

Fingerprint 2: The u and i zero crossings occur at the same instants.

Remark 2: Since $u = i/g$, then, if $i(t_*) = 0$ for some $t_* \geq 0$, then $u(t_*) = 0$ when $G_{min} < g(t_*) < \infty$. Therefore, to avoid the symbol 0/0, it suffices to show that the model (1),(2) yields the conductance $g(t_*) \neq 0$. See Fig.1(d) for an illustration.

Proof of fingerprint 2: If $i(t_*) = 0$ for some t_* , then, obviously, $i(t_*) < I_0$ and the hybrid arc model follows that of Mayr. Thus, from (3) we have $g(t_*) = g_M(t_*)$ and the g_M results from the Mayr model $g_M = G_{min} + i^2/P_0 - \theta dg_M/dt$. When $i(t) \rightarrow 0$, then we have $g_M(t) \rightarrow G_{min} + Ce^{-t/\theta}$. Since the $g(t)$ must be greater or equal G_{min} for small $i(t)$ (see a remark in section 1), therefore we must have that $C > 0$. This yields $g_M(t_*) \neq 0$. \diamond

Fingerprint 3: As $f \rightarrow \infty$, then the u - i pinched hysteresis characteristic becomes that of a memoryless resistor, meaning that the u - i graph is a single-valued one.

Remark 3: The third fingerprint can be proved, by analyzing the area enclosed by the hysteresis u - i as $f \rightarrow \infty$. Notice that f is the frequency of E in (2). We shall show that the enclosed area shrinks to zero as $f \rightarrow \infty$. This gives a single-valued relationship between u and i .

Proof of fingerprint 3: Since $E(t) = E_m \sin(2\pi ft)$ in (2) and the fact that $u(t)$ and $i(t)$ are periodic, we can assume that

$$\begin{aligned} u &= \sum_{k=1}^{\infty} [a_k \cos(2\pi fkt) + b_k \sin(2\pi fkt)] \\ i &= \sum_{k=1}^{\infty} [c_k \cos(2\pi fkt) + d_k \sin(2\pi fkt)] \end{aligned} \quad (5)$$

for some real numbers a_k, b_k, c_k and $d_k, k = 1, 2, \dots$

The area, say A , enclosed by the pinched hysteresis loop u - i over half period $t_* \leq t < t_* + T/2$, $T = 1/f$, equals

$$A = \oint u di = \int_{t_*}^{t_*+T/2} u(di/dt)dt. \quad (6)$$

Table 1: The $G_{min} + I_m^2/(2P_M)$ values for various frequencies.

f [kHz]	I_m [A]	$G_{min} + I_m^2/(2P_M)$ [S]
3	3.821	0.3650
5	2.264	0.1281
7	1.568	0.0615
9	1.152	0.0332
11	0.790	0.0156

Using (5) and $di/dt = (E - u - Ri)/L$ from (2) we obtain

$$\begin{aligned}
 A = & \frac{1}{L} \int_{t_*}^{t_*+T/2} \sum_{k=1}^{\infty} [a_k \cos(2\pi fkt) + b_k \sin(2\pi fkt)] \times \\
 & \{E_m \sin(2\pi ft) - \sum_{k=1}^{\infty} [a_k \cos(2\pi fkt) + b_k \sin(2\pi fkt)] \\
 & - R \sum_{k=1}^{\infty} [c_k \cos(2\pi fkt) + d_k \sin(2\pi fkt)]\} dt.
 \end{aligned} \tag{7}$$

Notice that the right-hand side of (7) contains integrals of various products of the cosine and sine terms. The integrals are computed over half of the period $T = 1/f$, that is for $t_* \leq t < t_* + T/2$. Such integrals can be computed according to the well-known formulas

$$\int_{t_*}^{t_*+T/2} p_k \sin(2\pi fkt) \times q_l \sin(2\pi flt) dt = \begin{cases} \frac{p_k q_k}{4f} & \text{for } k = l \\ 0 & \text{for } k \neq l \end{cases} \tag{8}$$

$$\begin{aligned}
 & \int_{t_*}^{t_*+T/2} p_k \cos(2\pi fkt) \times q_l \sin(2\pi flt) dt \\
 & = \begin{cases} 0 & \text{for } k = l \\ \frac{p_k q_l l [1 - \cos(\pi k) \cos(\pi l)]}{2\pi f(l^2 - k^2)} & \text{for } k \neq l \end{cases}
 \end{aligned} \tag{9}$$

In addition, the same right-hand side holds true if we replace both sine terms by cosine terms in (8).

Notice that by using the above integrals and the fact that $1/f$ is present in the non-zero right-hand sides in (8) and (9), we obtain the right-hand side of (7) in the form of an infinite series with each term proportional to $1/f$, reciprocal of frequency. Thus, if $f \rightarrow \infty$, then the area of the pinched hysteresis decays to zero. This means that the u - i characteristic becomes a single-valued one and the proof of the third fingerprint is complete. \diamond

Fig.1(c) indicates that when the frequency f increases, then the v - i characteristic not only becomes closer to a single-valued one, but it becomes a linear with decreasing values of g and i (assuming fixed value of E_m). The g is practically constant in Fig.1(c) for a particular large value of f . Note that since $i < I_0$ for large f values, therefore the Mayr model dominates in (1). One can estimate the constant value of g for large f , by using the well-known frequency formula for the Mayr model [30]. Namely, the sinusoidal current $i(t) = I_m \sin(2\pi ft)$ in the Mayr model yields $g(t) = G_{min} + \frac{I_m^2}{2P_M} \left\{ 1 + \frac{\cos(4\pi ft - \phi)}{\sqrt{1 + 16\pi^2 f^2 \theta^2}} \right\}$

with $\phi = \tan^{-1}(4\pi f\theta)$. Thus $\lim_{f \rightarrow \infty} g(t) = G_{min} + \frac{I_m^2}{2P_M}$. Fig.3 and the associated Table 1 illustrate the use of the above limit in a simple numerical example.

Comparing Fig.3(b) and Table 1 it is easy to notice that, with the increased frequency f , the $G_{min} + I_m^2/(2P_M)$ are indeed very good estimates of the *almost* constant g values. The last four values in the third column in Table 1 are marked on the vertical axis in Fig.3(b).

4 Variation of hystereses with parameters

Figs. 1(b) and 2(a) show various shapes of the hysteresis loops of (1),(2) when the frequency f and current I_0 change, respectively. Other parameters in the Cassie-Mayr model impact the hystereses, too. Fig. 4(a), 4(b) and 4(c) illustrate such an impact when the parameters K , L and U_C vary, respectively. The constant parameters in all three figures were: $\theta = 4 \times 10^{-4}$, $G_{min} = 10^{-8}$, $I_0 = 4.8$, $P_M = 20$, $R = 0.2$, $f = 50$ and $E_m = 75$. In addition, $U_C = 30$, $L = 10^{-3}$ and $K = \{0, 0.3, 1, 2, 5\}$ in Fig.4(a).

Also, $U_C = 30$, $K = 0.1$ and $L = \{5 \cdot 10^{-5}, 10^{-4}, 5 \cdot 10^4, 10^{-3}, 5 \cdot 10^{-3}\}$ in Fig.4(b). Finally, $K = 0.1$, $L = 10^{-3}$ and $U_C = \{1, 5, 10, 25, 50\}$ in Fig.4(c). The hysteresis loops are shown in the first quadrant only (positive voltage and current values). Symmetric graphs exist in the third quadrant with negative voltage and current values.

5 Conclusion

The seemingly distant and disjoint areas of electric arcs from welding, electric furnaces and circuit breakers on one side and memristors from nanometer electronics on the other side have been linked together through their identical mathematical properties (fingerprints). It was shown through mathematical analysis that the hybrid Cassie-Mayr model of electric arcs has all the fingerprints of memristors, passive nonlinear nanoelements with memory. By linking the electric arcs with memristors one can now apply various techniques and methods from the nanoscale electronics (i.e. to analyze energy and power [17],[28],[29]) to the nonlinear plasma phenomena in electric arc furnaces, circuit breakers and welding processes [4]-[7].

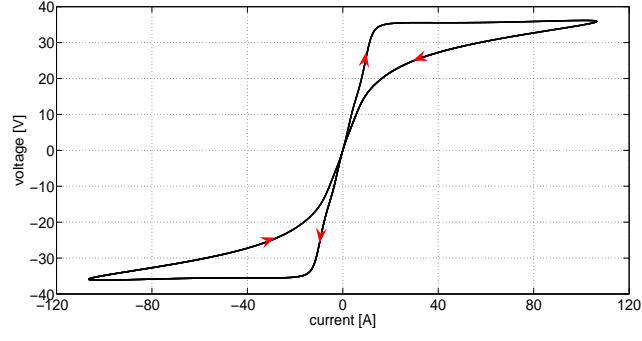
6 Acknowledgement

The author would like to thank Prof. Z. Trzaska from Warsaw (Poland) for his discussion on the topic of electric arcs.

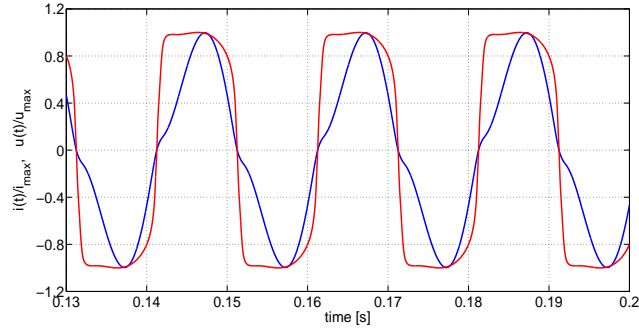
References

- [1] A. M. Cassie, Arc rupture and circuit severity: a new theory, Paris, CIGRE Rep. 102 (1939)
- [2] O. Mayr, Beitrage zur theorie des statischen und des dynamischen lichtbogens, Archiv für Elektrotechnik 37 (12) (1943) 588–608.
- [3] K.-J. Tseng, Y. Wang, D. M. Vilathgamuwa, An experimentally verified hybrid Cassie-Mayr electric arc model for power electronics simulations, IEEE Trans. Power Electronics 12 (3) (1997) 429–436.
- [4] M. Moghadasian, E. Al-Nasser, Modelling and control of electrode system for an electric arc furnace, 2nd Int. Conf. Research in Science, Engineering and Technology (ICRSET), pp. 129–133, March 21–22, 2014 Dubai (UAE) doi: 10.15242/IIE.E0314558.
- [5] S. Nitu, C. Nitu, C. Mihalache, P. Anghelita, D. Pavelescu, Comparison between model and experiment in studying the electric arc, J. Optoelectronics and Advanced Materials 10 (5) (2008) 1192–1196.
- [6] D. C. Bhonsle, R. B. Kelkar, New time domain electric arc furnace model for power quality study, J. Electr. Eng. 14 (3) (2014) 240–246.
- [7] A. Sawicki, L. Switon, R. Sosinski, Process simulation in the AC welding arc circuit using a Cassie-Mayr hybrid model, Supplement to the Welding Journal 90 (2011) 41s–44s.
- [8] M.L. Foucault, Experiments with the light of the voltaic arc, Journal of the Franklin Institute, 48 (1) 1849, 50–52.
- [9] E. Thomson, E. J. Houston, The electric arc – its resistance and illuminating power, Journal of the Franklin Institute, 108 (1) (1879) 48–51.
- [10] E. Karrer, The luminous efficiency of the radiation from the electric arc, Journal of the Franklin Institute, 183 (1) (1917) 61–72.
- [11] J. Slepian, The electric arc in circuit interrupters, Journal of the Franklin Institute, 214 (4) (1932) 413–442.
- [12] K.B. McEachron, Lightning protection since Franklin’s day, Journal of the Franklin Institute, 253 (5) (1952) 441–470.
- [13] D. S. Strukov, G. S. Snider, D. R. Stewart, R. S. Williams, The missing memristor found, Nature 453 (2008) 80–83.

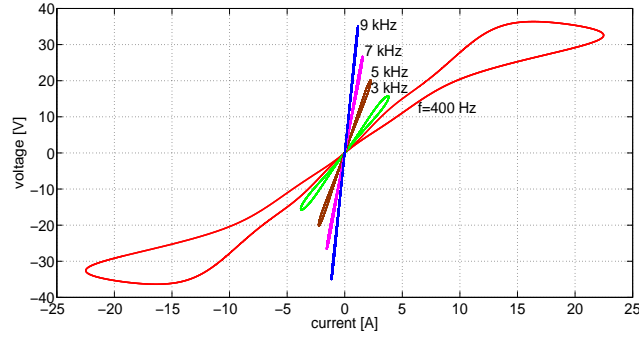
- [14] L. O. Chua, Memristor - the missing circuit element, *IEEE Trans. Circuit Theory* 18 (1971) 507–519.
- [15] L. O. Chua, K. Sung Mo, memristive devices and systems, *Proc. IEEE* 64 (1976) 209–223.
- [16] S. P. Adhikari, M. P. Sah, H. Kim, L. O. Chua, Three fingerprints of memristor, *IEEE Trans. Circuits and Systems-IL Regular Papers* 80 (11) (2013) 3008–021.
- [17] W. Marszalek, T. Amdeberhan, Least action principle for mem-elements, *J. Circ., Syst. & Comp.* 24 (10) (2015) 1550148.
- [18] M. P. Sah, H. Kim, L. O. Chua, Brains are made of memristors, *IEEE Circuits and Systems Magazine* 14 (1) (2014) 12–36.
- [19] D. Lin, S. Y. Ron Hui, L. O. Chua, Gas discharge lamps are volatile memristors, *IEEE Trans. Circuits and Systems-I: Regular Papers* 61 (7) (2014) 2066–2073.
- [20] S. Asapu, Y. V. Pershin, Electromechanical emulator of memristive systems and devices, *IEEE Trans. Electron Devices* 62 (11) (2015) 3678–3684.
- [21] W. Marszalek and Z. W. Trzaska, Memristive circuits with steady-state mixed-mode oscillations, *Electr. Lett.* 50 (2014) 1275–1277.
- [22] W. Marszalek and Z. W. Trzaska, Properties of memristive circuits with mixed-mode oscillations, *Electr. Lett.* 51 (2015) 140–141.
- [23] W. Marszalek, Bifurcations and Newtonian properties of Chua’s circuits with memristors, *DeVry Univ. J. of Scholarly Research* 2 (2) (2015) 13–21.
- [24] A. Sawicki, Assessment of power parameters of asymmetric arcs by means of the Cassie and Mayr models, *Electrical Review* 87 (2) (2011) 131–134.
- [25] D. Biolek, Z. Biolek, V. Biolkova, Pinched hysteretic loops of ideal memristors, memcapacitors and meminductors must be ‘self-crossing,’ *Electr. Lett.* 47 (25) (2011) 1385–1387.
- [26] Z. Biolek, D. Biolek, V. Biolkova, Analytical computation of the area of pinched hysteresis loops of ideal mem-elements, *Radioengineering* 22 (1) (2013) 32–35.
- [27] W. Marszalek, T. Amdeberhan, Memristive jounce (Newtonian) circuits, *Appl. Math. Modelling* (2015), doi: 10.1016/j.apm.2015.10.012.
- [28] W. Marszalek, On the action parameter and one-period loops of oscillatory memristive circuits, *Nonlinear Dynamics* 82 (1) (2015) 619–628.
- [29] H. Podhaisky and W. Marszalek, Bifurcations and synchronization of singularly perturbed oscillators: an application case study, *Nonlinear Dynamics* 69 (3) (2012) 949–959.
- [30] V. M. Myakishev, M. S. Zhevaev, E. M. Shishkov, A method for determining the time constant of a welding arc, *Russian Electrical Engineering*, 80 (2) (2009) 78–80.



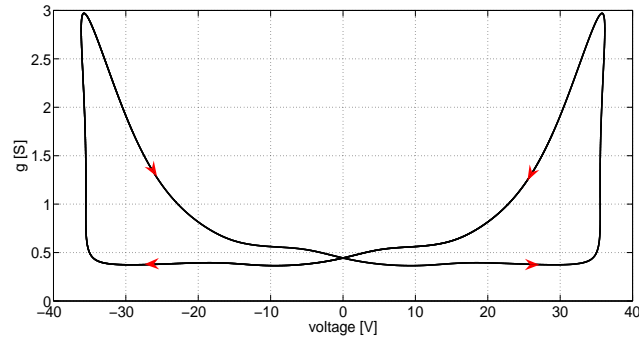
(a) Pinched hysteresis for $f = 50$ Hz.



(b) Normalized $u(t)$ — and $i(t)$ — for $f = 50$ Hz.

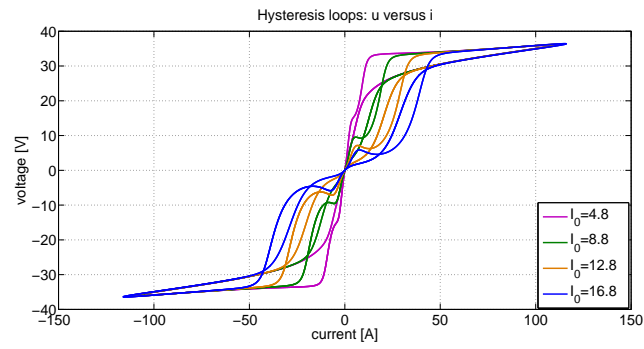


(c) Pinched hystereses for $f = \{0.4, 3, 5, 7, 9\}$ kHz.

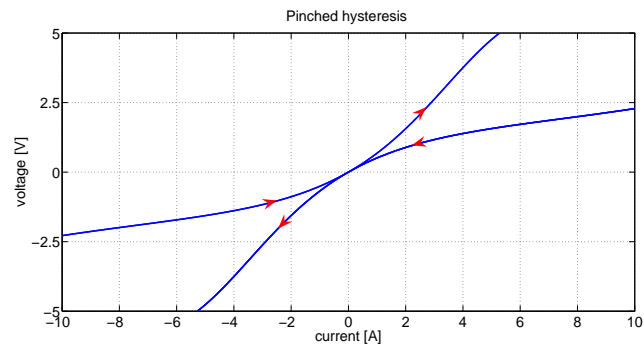


(d) Conductance g versus voltage u for $f = 50$ Hz.

Figure 1: Solution of (1),(2) with $u = i/g$. (a)-(c): the three fingerprints of the Cassie-Mayr model; (d) conductance g versus voltage u . Parameters $\theta = 4 \times 10^{-4}$, $G_{min} = 10^{-8}$, $I_0 = 4.8$, $P_M = 20$, $U_C = 30$, $R = 0.2$, $L = 10^{-3}$, $K = 10^{-1}$, $E_m = 75$. The *ode45* solver from Matlab with $abserr=relerr=10^{-10}$ was used.

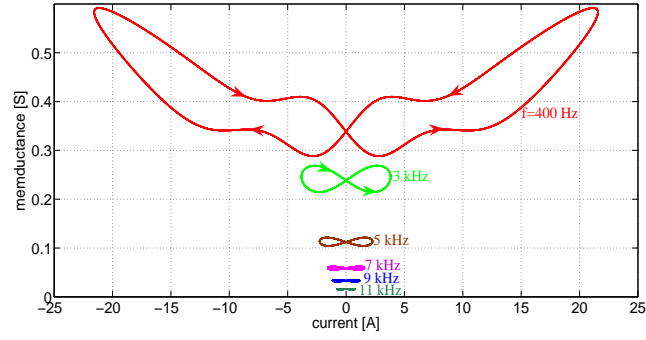


(a) Pinched hystereses for different I_0 values.

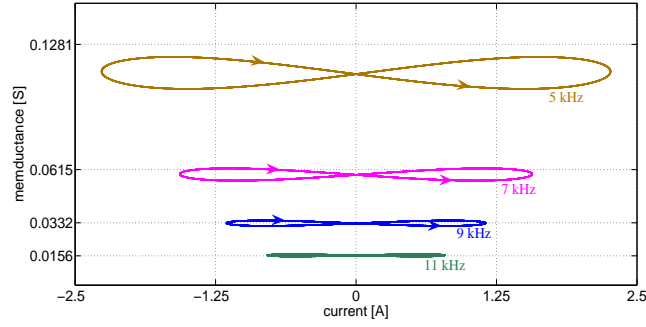


(b) Motion around $(0, 0)$ for $I_0 = 16.8$.

Figure 2: Various pinched hystereses.

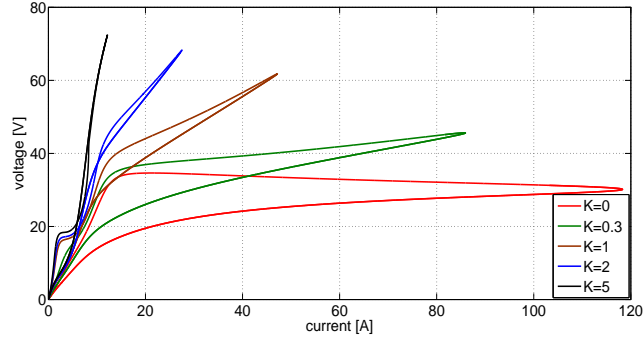


(a) The g - i loops for $f = \{0.4, 3, 5, 7, 9, 11\}$ kHz.

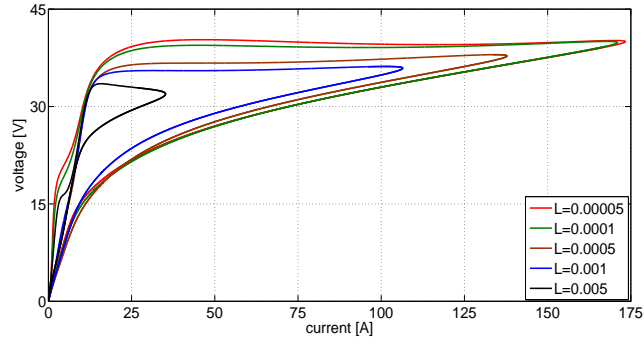


(b) Enlargements of the g - i loops for $f = \{5, 7, 9, 11\}$ kHz in Fig.3(a).

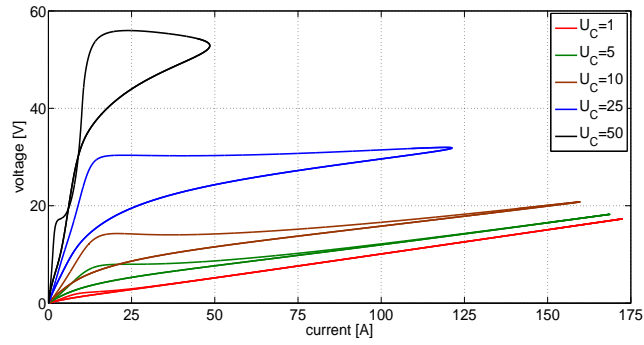
Figure 3: The g - i loops for various values of f in $E(t)$ and $\theta = 2 \cdot 10^{-4}$, $K = 0.5$. Other parameters as given in Fig.1.



(a) Hysteresis loops for various values of K .



(b) Hysteresis loops for various values of L .



(c) Hysteresis loops for various values of U_C .

Figure 4: Impact of parameters K , L and U_C on the pinched hysteresis loops of the Cassie-Mayr model (1),(2). The *ode45* solver from Matlab with $abserr=relerr=10^{-10}$ was used.